

Millikelvin de Haas–van Alphen and magnetotransport studies of graphite

S. B. Hubbard, T. J. Kershaw, A. Usher, A. K. Savchenko,* and A. Shytov

School of Physics, University of Exeter, Stocker Road, Exeter EX4 4QL, United Kingdom

(Received 15 July 2010; revised manuscript received 12 October 2010; published 20 January 2011)

Recent studies of the electronic properties of graphite have produced conflicting results regarding the positions of the different carrier types within the Brillouin zone, and the possible presence of Dirac fermions. In this paper we report a comprehensive study of the de Haas–van Alphen, Shubnikov–de Haas, and Hall effects in a sample of highly orientated pyrolytic graphite, at temperatures in the range 30 mK to 4 K and magnetic fields up to 12 T. The transport measurements confirm the Brillouin-zone locations of the different carrier types assigned by Schroeder, Dresselhaus, and Javan, *Phys. Rev. Lett.* **20**, 1292 (1968): electrons are at the K point, and holes are near the H points. We extract the cyclotron masses and scattering times for both carrier types from the temperature- and magnetic-field-dependences of the magneto-oscillations. Our results indicate that the holes experience stronger scattering and hence have lower mobility than the electrons. We utilize phase-frequency analysis and intercept analysis of the $1/B$ positions of magneto-oscillation extrema to identify the nature of the carriers in graphite, whether they are Dirac or normal (Schrödinger) fermions. These analyses indicate normal holes and electrons of indeterminate nature.

DOI: [10.1103/PhysRevB.83.035122](https://doi.org/10.1103/PhysRevB.83.035122)

PACS number(s): 71.20.-b, 71.18.+y, 81.05.U-

I. INTRODUCTION

Graphite is a fascinating material whose novel electronic properties have been extensively studied.¹ It consists of weakly-bonded layers of graphene, resulting in a highly anisotropic Fermi surface and semimetallic properties. Recently there has been a resurgence of interest in graphite due to the possible occurrence of quasirelativistic graphene physics in this 3D bulk material. There is however much discussion over whether the Dirac fermions found in graphene are actually present in graphite samples.²⁻⁸

Tight-binding calculations using a 2D model of graphite were originally utilized by Ref. 9 (SW) in 1958. They introduced the first 3D model of graphite, a $\mathbf{k} \cdot \mathbf{p}$ perturbation calculation using the tight-binding wave functions of the 2D model as basis functions. The result was a band structure dependent on seven parameters (γ_0 to γ_5 and Δ) to be determined experimentally.

Table I summarizes the results of subsequent studies of the band structure of graphite, which utilize magneto-oscillatory effects such as the de Haas–van Alphen (dHvA) and Shubnikov–de Haas (SdH) effects. Table II lists the theoretical expectations for these results, as will be discussed later in this section. Reference 10 used an interpretation of previous measurements of the dHvA effect in single-crystal natural graphite^{11,12} to determine, or place limits on, the SW parameters. He derived a Fermi surface of the form of three approximately ellipsoidal surfaces along the HKH edge of the Brillouin zone. This analysis was unable to specify the parameter γ_2 , determining the carrier types (electrons or holes) at the three extremal orbits, but favored the assignment of holes to the extremal orbit at K and electrons to the extremal orbits close to H . Figure 1 shows the Brillouin zone of graphite with the ellipsoidal Fermi surfaces along the HKH edges. Note that in the figure the carrier labeling reflects that of the current accepted associations from the work of Ref. 13, which contradict the original assignments.¹⁰

Subsequently, Ref. 14 used angle-dependent SdH measurements on single-crystal natural graphite to demonstrate that the Fermi surfaces for both holes and electrons are closed. They

found that the extremal cyclotron orbit at the K point is larger than the orbit near the H point.

The authors of Ref. 15 were the first to consider the phase of the magneto-oscillations. They followed the formula of Ref. 16 from which the fundamental harmonic of the oscillatory magnetic susceptibility can be written as

$$\Delta\chi \propto \cos\left(2\pi\left[\frac{B_0}{B} - \gamma + \delta\right]\right), \quad (1)$$

where B_0 is the fundamental frequency of the magneto-oscillations for a given carrier type, and B is the applied magnetic field. The phase factor γ comes from the Onsager–Lifshitz quantization condition and is $\frac{1}{2}$ for nonrelativistic free electrons. The offset δ is related to the curvature of the Fermi surface in the k_z direction, and is $-\frac{1}{8}$ or $+\frac{1}{8}$ for maximum or minimum extremal cross sections, respectively. Reference 15 showed that, according to the SW model, γ takes on its usual value of $\frac{1}{2}$ at the K point of the Brillouin zone, but is zero at the H points. However, at the positions of both the extremal orbits (K , and $\sim 70\%$ of the way from K to H)¹⁰ the SW model predicts $\gamma = \frac{1}{2}$ —a result with which their experimental dHvA results agreed. Reference 15 also pointed out a fundamental difficulty in measuring the phase: one needs to approach the quantum limit of low Landau-level filling factors in order to obtain accurate results, but in this limit the oscillations cease to be periodic in $1/B$.

In 1968, the magnetoreflexion studies of Ref. 13 led to a reassessment of the SW band parameters, with the conclusion that the majority carrier types assigned previously were incorrect. It was shown that *electrons* occupy the orbits at the K point while *holes* occupy those near the H point (as shown in Fig. 1). This was confirmed by the magnetoresistance, Hall effect, thermopower, and thermal resistivity measurements of Ref. 17.

In 2004, individual layers of graphene were first isolated,¹⁸ stimulating an explosion of interest in the material. Experiments have shown that the charge carriers in graphene are massless, quasirelativistic Dirac fermions (DFs) with a linear dispersion relation resulting in an anomalous quantum Hall

TABLE I. Comparison of the conclusions of studies of the carriers' locations within the Brillouin zone and their natures in graphite. f_{FFT} is the frequency of the $1/B$ oscillations for each carrier type. The phases δ and γ are defined in the text. The natures of the carriers, whether they are Schrödinger or Dirac fermions (SF or DF) and whether they are three- or two-dimensional (3D or 2D), are summarized for each study. In the case of Williamson, the authors did not discuss carrier natures, but their phases are consistent with the interpretations stated. In some other cases authors' conclusions are not consistent with the phases measured. These are marked (*) and discussed in the text.

First Author	Material studied	Technique used	Low frequency			High frequency		
			f_{FFT} (T)	Carrier, location	Total phase, $\varphi = (\delta - \gamma) [2\pi]$	f_{FFT} (T)	Carrier, location	Total phase, $\varphi = (\delta - \gamma) [2\pi]$
McClure ¹⁰	–	dHvA theory	–	electrons near H	–	–	holes K	–
Soule ¹⁴	Natural	Angle-dependent SdH	4.8	electrons near H	–	6.7	holes K	–
Williamson ¹⁵	Pyrolytic	dHvA	4.8 ± 0.3	electrons near H	0.38 ± 0.05 3D SF	6.6 ± 0.4	holes K	0.32 ± 0.09 3D SF
Schroeder ¹³	Pyrolytic	Polarized magnetoreflexion	–	holes near H	–	–	electrons K	–
Woollam ¹⁷	Pyrolytic	SdH, Hall effect, thermopower and thermal resistivity	4.9 ± 0.1	holes near H	–	6.2 ± 0.3	electrons K	–
Luk'yanchuk ²	HOPG	dHvA and SdH	4.68	electrons	0.375 3D SF	6.41	holes	0.5 2D DF*
Luk'yanchuk ³	HOPG	SdH	4.68	electrons	0.5 3D SF*	6.41	holes	0 2D DF
Mikitik ⁴	–	Reanalysis of Ref. 2	–	holes near H	0.375 3D SF	–	electrons K	0.5 3D SF*
Schneider ⁶	Natural and HOPG	SdH	4.51 ± 0.05	holes near H	-0.43 ± 0.05 3D SF* -0.52 ± 0.05 2D SF	6.14 ± 0.05	electrons K	-0.28 ± 0.05 3D SF* -0.46 ± 0.05 2D SF
This paper:	HOPG	dHvA, Hall and SdH	4.36 ± 0.05	holes near H	-0.48 ± 0.06 2D SF	5.97 ± 0.01	electrons K	-0.20 ± 0.05 indeterminate

effect with plateaus at half-integer filling factors.^{19,20} In the same year, Refs. 2 and 3 reported 2D-like electronic properties in highly oriented pyrolytic graphite (HOPG) and have claimed also to have observed the presence of DFs. Reference 2 presented dHvA and SdH experiments on a sample of HOPG at a temperature of 2 K using magnetic fields up to 9 T. They determined the nature of the carriers, either massless DFs or massive Schrödinger fermions (SFs, also described in the literature as “normal” fermions), by two-dimensional phase-frequency analysis of the complex Fourier transforms of the quantum oscillations. Table II details the values of the phases γ and δ from Eq. (1) expected for carriers of different nature (DF or SF) and dimensionality (2D or 3D). They concluded that the high-frequency carriers (which they

TABLE II. Phases γ and δ from Eq. (1) for different carrier natures: Schrödinger or Dirac fermions (SF or DF); two- or three-dimensional (2D or 3D).

Nature	$\gamma [2\pi]$	$\delta [2\pi]$	Total phase $\varphi = (\delta - \gamma) [2\pi]$
3D SF	± 0.5	-0.125	$+0.375, -0.625$
2D SF	± 0.5	0	$+0.5, -0.5$
3D DF	0	-0.125	$+0.875, -0.125$
2D DF	0	0	0

assigned to be holes) are 2D DFs and the low-frequency carriers (which they assigned to be electrons) are 3D SFs. In this terminology the conclusion of the previous studies of Ref. 15 were that both carrier types were 3D SF, raising a controversy over the nature of the high-frequency carriers. Luk'yanchuk and Kopelevich² assigned the carrier types in contradiction to Schroeder *et al.*¹³ and Woollam.¹⁷

In 2006, Ref. 3 detailed further SdH experiments under similar conditions. The carriers were again assigned in contradiction to Refs. 13 and 17. Plotting the extrema of the oscillations against Landau-level index, the total phase ($\delta - \gamma$) for each carrier type was found using the equation

$$\Delta\sigma_{xx}(B) \simeq A(B) \cos\left(2\pi \left[\frac{B_0}{B} - \gamma + \delta\right]\right), \quad (2)$$

where $\Delta\sigma_{xx}$ is the oscillatory part of the longitudinal conductivity and $A(B)$ is the nonoscillatory amplitude. Hence the carrier nature and dimensionality was deduced from Table II. The conclusion was in agreement with the previous letter of Luk'yanchuk and Kopelevich²: they found that the high-frequency carriers (which were assigned to be holes) are 2D DFs and the low-frequency carriers (which were assigned to be electrons) are 3D SFs. This intercept analysis method can also be applied to dHvA oscillations through Eq. (1).

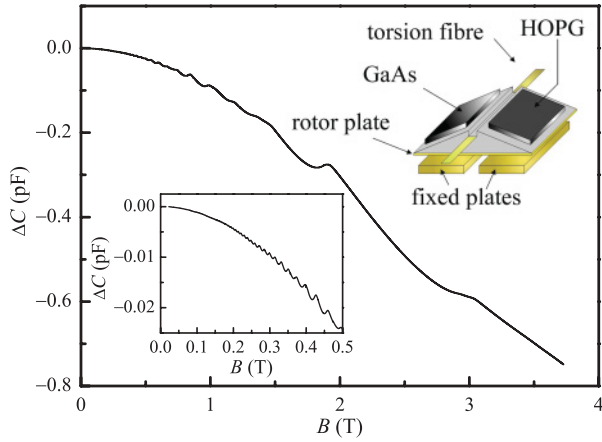


FIG. 3. (Color online) Raw magnetometry data (change in magnetometer capacitance vs magnetic field) measured at 30 mK. The lower left inset shows the detail at low magnetic fields. The upper inset is a schematic picture of the millikelvin torsion-balance magnetometer. The sample magnetisation causes a twist of the rotor which results in an imbalance in the differential capacitor formed by the fixed and rotor plates.

same sample of HOPG, covering a broader range of magnetic fields and temperatures than previous studies.

II. EXPERIMENTAL DETAILS

The sample used for the experiments detailed in this paper was a piece of ZYB grade HOPG (mosaic spread, $0.8 \pm 0.2^\circ$; purity, 99.99%; room-temperature resistivity parallel to the graphene planes, $4 \times 10^{-7} \Omega \text{ m}$; room-temperature resistivity perpendicular to the graphene planes, $2 \times 10^{-3} \Omega \text{ m}$; room-temperature resistivity ratio, 5×10^3) measuring $10 \times 5.5 \times 0.5 \text{ mm}$. Magnetization measurements were made using a torsion-balance magnetometer shown schematically in the inset of Fig. 3 and described in detail by Ref. 21. The graphite sample had the normal to its atomic planes tilted, in two separate experiments, at 2° and at 20° to the applied magnetic field. The magnetometer rotor was balanced using a piece of semi-insulating GaAs of similar mass. Subsequently, the Hall and SdH measurements were performed on the same sample, contacted using silver paint, in six-terminal Hall-bar geometry. Standard low-frequency AC techniques were used with currents below $10 \mu\text{A}$. Measurements were carried out at temperatures in the range 30 mK to 3.8 K in the mixing chamber of a low-vibration dilution refrigerator. The superconducting magnet used was found to have a remanent field of 26 mT, which has been subtracted from all the results presented. This remanent field was determined by analyzing the (well-understood) dHvA oscillations in a GaAs hetero-junction, and confirmed using a Hall-probe measurement.

III. RESULTS

A. Hall effect

Figure 4 shows the Hall resistance R_{xy} as a function of magnetic field at 30 mK. A large R_{xx} signal, caused by imperfect contact geometry, was removed by subtracting the Hall resistances measured in forward and reverse magnetic fields.

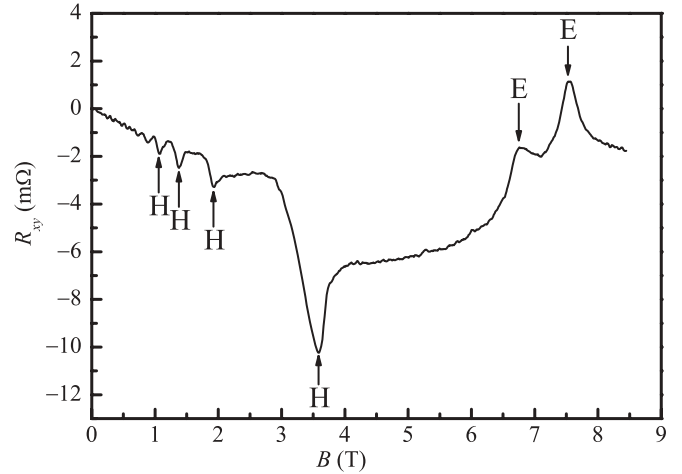


FIG. 4. Hall resistance R_{xy} plotted as a function of magnetic field at 30 mK. Downward pointing features (marked H) occur when the Fermi energy passes through hole Landau levels; upward ones (E) occur when the Fermi energy passes through electron Landau levels.

The oscillations in R_{xy} may be explained as follows. When the Fermi energy passes through a hole (electron) Landau level, scattering is enhanced and μ_h (μ_e) is reduced causing a downward (upward)-pointing feature in R_{xy} . Thus all the dips below 4 T are due to hole Landau levels, while the twin peaks near 7.5 T are caused by a spin-split electron Landau level. This interpretation is in agreement with that of Ref. 17 and enables us to confirm that the carriers with the higher oscillation frequency (higher value of B_0) are electrons while those with the lower frequency are holes (contrary to the assertion of Ref. 2).

B. De Haas–van Alphen effect

A typical plot of magnetic susceptibility vs $1/B$, taken at 30 mK is shown in Fig. 5. The magnetic field in this and subsequent figures is the component of the applied field perpendicular to the graphite planes. The magnetometer was calibrated *in situ* using the known electrostatic force between

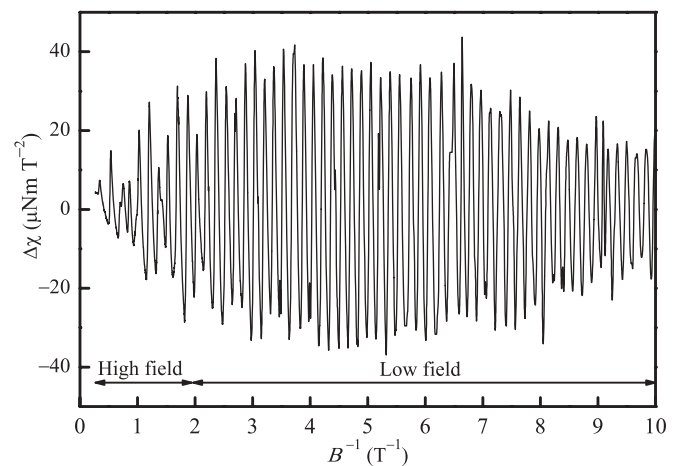


FIG. 5. Oscillatory magnetic susceptibility $\Delta\chi$ as a function of inverse magnetic field at 30 mK. The arrows indicate the ranges of B^{-1} used to obtain the FFTs of Fig. 6.

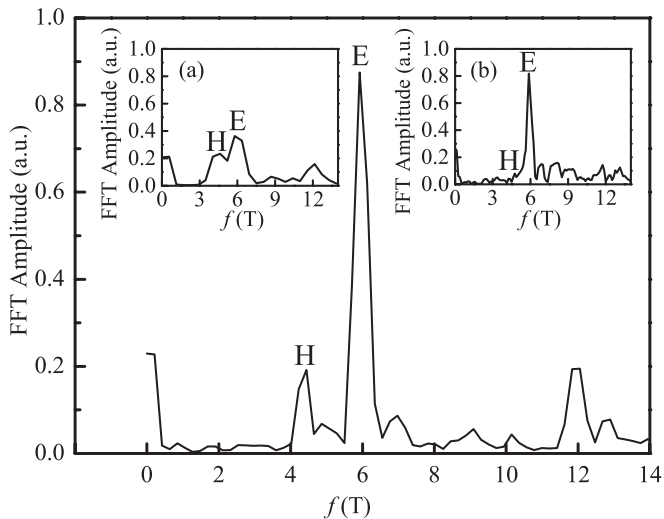


FIG. 6. FFT of the 30 mK magnetic susceptibility (Fig. 5) using data in the range from 0.27 T^{-1} to 5 T^{-1} , showing the presence of hole oscillations with a fundamental field of 4.36 T, marked ‘H’, and electron oscillations of approximately 5.97 T, marked ‘E’. The second harmonics of the two carriers are also visible at twice their fundamental frequencies. To illustrate the magnetic field dependences of the two sets of oscillations, the inset (a) shows the FFT from 0.27 T^{-1} to 2 T^{-1} (‘High field’ on Fig. 5) where hole and electron peaks have roughly equal amplitude, while inset (b) shows the FFT for the data range from 2 T^{-1} to 10 T^{-1} (‘Low field’ on Fig. 5) demonstrating the dominance of the electron oscillations at low B .

the capacitor plates,²² and the raw capacitance data (Fig. 3) converted to torque and hence to magnetic moment, using $\tau = \mathbf{m} \times \mathbf{B}$. The magnetic moment is converted to magnetisation and then differentiated to give magnetic susceptibility. The data in the figure have been filtered to remove high-frequency noise. However, all the analysis presented in this paper has been carried out on unfiltered data. The fast Fourier transform (FFT) algorithm used later requires that the susceptibility vs $1/B$ data be interpolated to an integer power of 2, in this case 2^{14} points.

1. Magnetic-field and temperature dependences

Figure 6 shows the FFT of the 30 mK magnetic susceptibility data from 0.27 T^{-1} to 5 T^{-1} . Over this field range, both hole oscillations (FFT peak 4.36 T, marked H) and electron oscillations (5.97 T, marked E) are visible, as well as their second harmonics. The insets show the FFT amplitudes for the high-field [(a), from 0.27 T^{-1} to 2 T^{-1}] and low-field [(b), from 2 T^{-1} to 10 T^{-1}] ranges, respectively. In the high-field FFT both peaks are of roughly equal height, whereas in the low-field FFT, the electron peak dominates. These data demonstrate that the (low-frequency) hole oscillation amplitude reduces more rapidly with decreasing field than that of the electrons. This implies either that the hole Landau levels are more closely spaced than the electron ones (the cyclotron masses satisfy the condition $m_h > m_e$), or that holes are more strongly scattered than electrons.

In order to distinguish between these two interpretations, we have examined the temperature dependence of the dHvA oscillations in Fig. 7. The oscillations at high $1/B$, which are predominantly due to electrons, diminish rapidly as

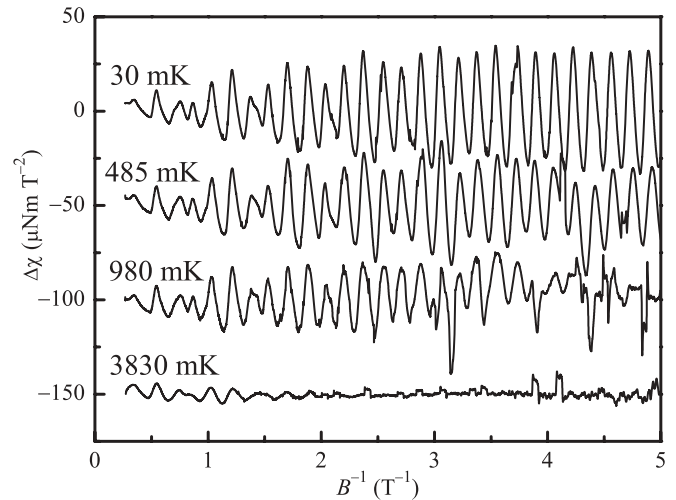


FIG. 7. dHvA oscillations at a range of temperatures. Oscillations at high B^{-1} are predominantly due to electrons and these disappear rapidly as temperature increases leaving only the hole oscillations at low B^{-1} . Traces for successive temperatures are offset for clarity.

temperature increases, while the oscillations at low $1/B$ (holes) remain. This is shown explicitly in the FFTs of these data, in Fig. 8. The fact that hole oscillations are more robust to temperature than those of electrons rules out the suggestion above that the hole Landau levels are more closely spaced than those of the electrons, and indeed indicates that the opposite is the case, $m_h < m_e$. The observation that the high frequency carriers have larger mass than the low frequency ones is in agreement with Ref. 14 which found cyclotron masses of $0.039 m_0$ and $0.057 m_0$ for the low-frequency and high-frequency carriers, respectively (although they assigned the wrong carrier types to these, as discussed above). Thus the only possible interpretation of Fig. 6 is that the holes experience stronger scattering.

Various effects could cause different scattering rates for holes and electrons. The scattering rate is determined by the integral of the density of states over the Fermi surface and

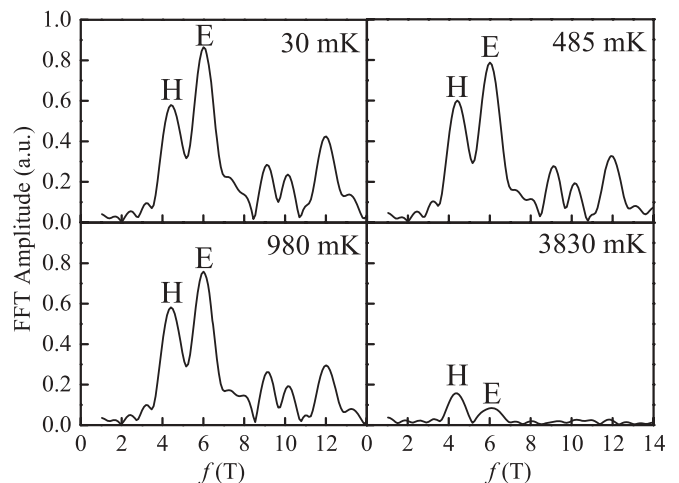


FIG. 8. FFT plots of the dHvA oscillations using data in the range from 0.27 T^{-1} to 2 T^{-1} , for a range of temperatures. The high-frequency (electron, E) peak is suppressed more rapidly with temperature than the low-frequency (hole, H) peak.

the different densities of states for electrons and holes, caused by the different shapes of the Fermi surface at the K point and near the H points, will give different rates. The different natures of the carriers, DF or SF, also affect scattering. It is known that in graphene and carbon nanotubes the chiral nature of the DFs suppresses back-scattering.²³ Further experiments on different types of graphite would help to clarify the causes of this effect.

We can obtain quantitative information about the carrier effective masses and about scattering, from an analysis of the damping of the oscillations in magnetization with magnetic field and temperature. The amplitude of the magnetisation oscillations is given by

$$\Delta M \propto \frac{\chi}{\sinh \chi} \exp\left(-\frac{\pi}{\omega_c \tau_q}\right), \quad (3)$$

where $\chi = 2\pi^2 k_B T / \hbar \omega_c$, $\omega_c = eB/m^*$, and τ_q is the quantum lifetime. Determining τ_q is only possible for the carrier whose oscillations are dominant, in this case electrons. We

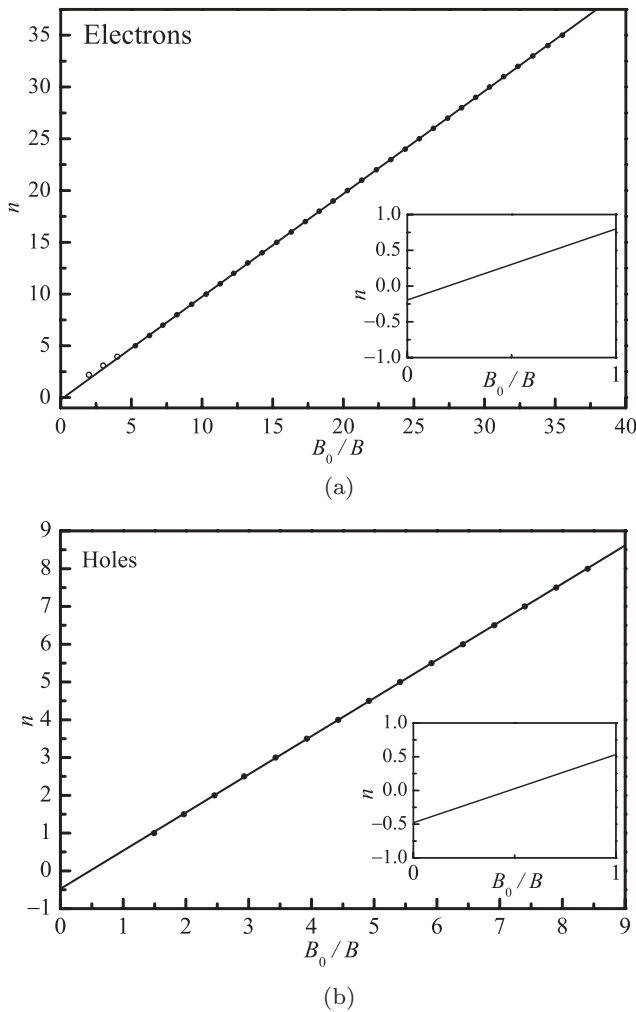


FIG. 9. Intercept phase analysis of the 30 mK dHva oscillations. (a) Analysis of the oscillations of electrons. Peak position vs Landau-level index n is plotted up to 5 T^{-1} . The intercept (see inset) indicates a phase of $-0.20 \pm 0.05 [2\pi]$. The open circles show how the low-index raw data deviate from the straight line. (b) Analysis of the hole oscillation extrema (peaks and troughs) indicating a phase of $-0.48 \pm 0.06 [2\pi]$, consistent with 2D SFs.

find that, for electrons, $m^* = 0.046 \pm 0.003 m_0$ and $\tau_q = 1.7 \pm 0.1 \times 10^{-12} \text{ s}$. This effective mass is somewhat lower than the value reported by Ref. 14. If we assume that τ_q is the same as the momentum relaxation time (the assumption of short-range scattering) then we obtain a mobility $\mu_e = 6.7 \pm 0.4 \text{ m}^2(\text{V s})^{-1}$.

2. Carrier natures—phase analysis

From the peaks in the FFT amplitudes the fundamental fields for the charge carriers have been identified. They are: low-frequency holes at $4.36 \pm 0.05 \text{ T}$ and high frequency electrons at $5.97 \pm 0.01 \text{ T}$. Following the approaches of Refs. 2 and 6, we can also extract the phase of the oscillations to determine the nature of the two types of carrier—whether they are DFs or SFs. Two types of analysis can be applied: a plot of the $1/B$ positions of the oscillation extrema vs Landau-level index yields an intercept from which the phase can be extracted; and the phase can be obtained directly from the FFT.

The phase is to be obtained using Eq. (1) which applies to the fundamental frequency of the susceptibility oscillations. Since the raw data are not sinusoidal, they need to be filtered in order to perform an intercept analysis. Fourier filtering was used, with a pass band centered approximately on the peak frequencies obtained from the FFT, and a band width sufficiently narrow to exclude the other peaks in the FFT. Various combinations of band width and center were tested, as well as other filter methods, and the intercept results were found to be fairly insensitive to these choices.

Figure 9 shows the results of intercept phase analysis for the 30 mK data of Fig. 5. Low-index oscillation extrema (up to $n = 4$) in the raw data (open circles) are shown in the electron plot (a) to illustrate the deviation which has been commented upon by Refs. 6 and 24, but are not used in the fit. No such deviation is apparent in the hole data. An intercept of zero corresponds to a total phase of zero (2D DFs from Table II), while an intercept of -0.5 corresponds to a total phase of $-\pi$ (2D SFs). The results are summarized in Table III. From Fig. 9, the intercepts (in units of 2π) are: for electrons, -0.20 ± 0.05 , not consistent with any of the assignments in Table II; for holes, -0.48 ± 0.06 , consistent with their assignment as 2D SFs. The error bars quoted for these intercepts reflect both the scatter of the straight-line graphs and small changes in intercept dependent on filtering parameters.

Phase information was also extracted directly from the FFTs. The phase was found to vary rapidly with field close to the FFT peaks (Fig. 10), and consequently the uncertainty in the phase was governed by the accuracy with which one could determine the peak positions, which in turn was controlled by the range in $1/B$ of the susceptibility data. With the data spacing of Fig. 10 we estimate the uncertainty in the position of the FFT peak to be about $\pm 0.1 \text{ T}$ leading to an error in the phase of about $\pm \pi/2$. Consequently, this gives a reasonable indication of carrier nature, but is not sufficiently accurate to determine dimensionality. Nevertheless the results of this method are in very good agreement with those of the intercept method (Table III): the phases (in units of 2π) are: for electrons, -0.25 ± 0.25 , the error bar being too large to determine the nature of the carriers; for holes, -0.45 ± 0.25 , consistent with their assignment as SFs.

TABLE III. Experiment conclusions for the nature of carriers in graphite.

Carrier	Fundamental field (T)	Total phase from $\Delta\chi$ ($\delta - \gamma$) [2π]		Total phase from $\Delta\sigma_{xx}$ ($\delta - \gamma$) [2π]		Outcome
		Intercept	FFT	Intercept	FFT	
Electrons	5.97 ± 0.01	-0.20 ± 0.05	-0.25 ± 0.25	–	–	indeterminate
Holes	4.36 ± 0.05	-0.48 ± 0.06	-0.45 ± 0.25	-0.48 ± 0.01	-0.49 ± 0.25	2D SF

C. Shubnikov–de Haas effect

Figure 11 shows the dependence of the longitudinal resistance R_{xx} on magnetic field. Drude theory predicts a quadratic dependence of R_{xx} on B at low fields, as observed in the inset to Fig. 11. Under the assumption of equal carrier densities the Drude model predicts

$$\frac{R_{xx}(B)}{R_{xx}(0)} = 1 + \mu_e \mu_h B^2, \quad (4)$$

from which we obtain $\mu_e \mu_h = 7.3 \text{ m}^4 (\text{Vs})^{-2}$, which we will compare with the mobilities obtained from the field-dependent amplitudes of the dHvA and SdH oscillations below. It should be noted that relaxing the assumption of equal carrier densities does not change this value significantly for reasonable carrier-density differences.

Figure 12 represents the oscillating part of σ_{xx} , $\Delta\sigma_{xx}$, as a function of $1/B$ at a temperature of 30 mK. The quantity plotted, $-\Delta R_{xx}$, is proportional to $\Delta\sigma_{xx}$ through the relationship

$$\Delta\sigma_{xx} = \Delta \frac{\rho_{xx}}{\rho_{xx}^2 + \rho_{xy}^2} \simeq -\frac{\Delta\rho_{xx}}{\rho_{xx}^2} \sim -\Delta R_{xx}. \quad (5)$$

The oscillations above 0.25 T^{-1} correspond to those seen in the Hall effect, which have been identified as hole oscillations. Only the two features around 0.14 T^{-1} (7 T) are associated with electrons. The FFT of $-\Delta R_{xx}$ (inset to Fig. 12) shows a clear peak due to hole oscillations but no evidence of electrons. This is consistent with the lack of electron-related features in the raw data, but contrasts with the analysis of the susceptibility data.

To understand the absence of electrons in the SdH data, we note the following. For a conductor with only one carrier type, the SdH oscillations and dHvA oscillations are both related

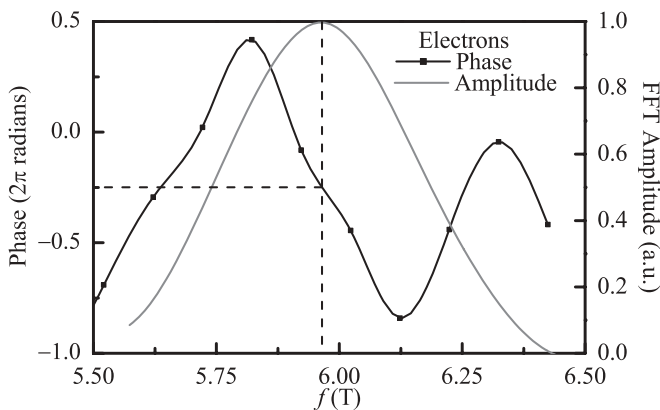


FIG. 10. FFT phase analysis of the 30 mK dHvA results for electrons—a phase of $-0.25 \pm 0.25 [2\pi]$ is observed. The error arises from the uncertainty in determining the peak position.

to the oscillations in the density of states, and are therefore proportional to each other (see, e.g., Section 11.1 of Ref. 25):

$$\frac{\delta\sigma_{xx}}{\sigma_{xx}} \sim \left(\frac{m^* B_0}{B} \right)^2 \frac{\partial M}{\partial B}, \quad (6)$$

where m^* is the cyclotron mass, and B_0 is the fundamental field. Note that the oscillating correction to the conductivity is proportional to the conductivity itself. The latter is inversely proportional to the mobility in strong fields: $\sigma_{xx} \propto 1/(\mu B^2)$. Therefore, the amplitude of conductivity oscillations at high fields, when the Dingle factor can be neglected, is higher if the mobility is *lower*. This is because, while thermodynamic dHvA oscillations are entirely determined by the density of states, SdH oscillations are caused by the enhancement of the scattering rate by the peaks in the density of states. For this reason, they also include the scattering rate as a prefactor.

In graphite, different carrier types contribute independently to conductivity oscillations. The relative magnitude of such contributions depends on the scattering rate for a given carrier type. Thus, high-mobility electrons should contribute *less* to the SdH oscillations than low-mobility holes.

Figure 12(b) shows the intercept phase analysis for the SdH data. The SdH data have significant harmonic content in the range over which the analysis is carried out as can be seen from their FFT [inset of Fig. 12(a)]. The same filtering process as described for the dHvA data above was used to obtain extrema positions in Fig. 12(b). The raw extrema are shown for comparison. A phase of $-0.48 \pm 0.01 [2\pi]$ is in excellent agreement with the analysis of the dHvA data [Fig. 12(b)] once

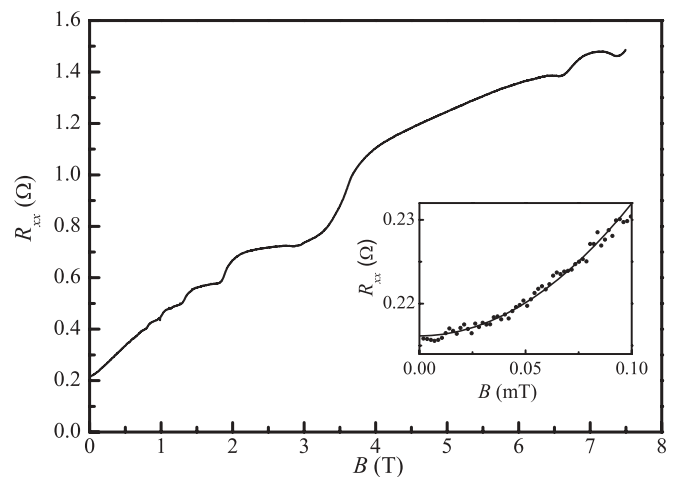


FIG. 11. R_{xx} as a function of magnetic field at 30 mK. The inset shows the quadratic dependence of R_{xx} at low magnetic fields predicted by the Drude model, from which the product of the electron and hole mobilities may be deduced.

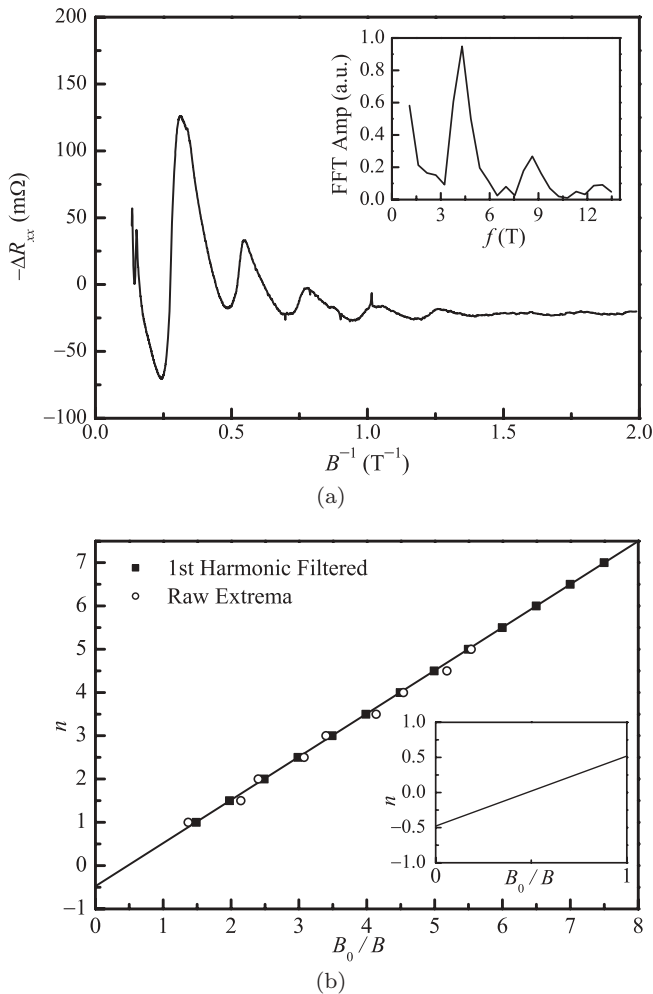


FIG. 12. (a) $-\Delta R_{xx}$ (proportional to $\Delta\sigma_{xx}$) as a function of inverse magnetic field at 30 mK. The inset is the FFT; the low frequency (hole) peak and its first harmonic are visible but the high frequency (electron) peak is not. (b) Intercept phase analysis of the SdH oscillation extrema (peaks and troughs). Only holes could be analysed and first-harmonic filtered data were used as discussed in the text, yielding a phase of $-0.48 \pm 0.01 [2\pi]$, consistent with 2D SF carriers. Raw extrema are also shown but exhibit systematic shifts to the right and to the left of the filtered data due to the presence of higher harmonics.

again identifying the holes as 2D SFs. FFT phase analysis of the SdH data yields a hole phase of $-0.49 \pm 0.25 [2\pi]$. This is in agreement with the intercept phase and the phases from the dHvA analysis, and indicates that holes are SFs, but again is subject to a substantial error.

The amplitude ΔR_{xx} of the resistivity oscillations has the same magnetic field and temperature dependences as ΔM

[Eq. (3)]. Analysis of this amplitude gives, for holes, $m^* = 0.033 \pm 0.003 m_0$ and $\tau_q = 2.1 \pm 0.2 \times 10^{-13}$ s. This effective mass is in reasonable agreement with the value reported by Ref. 14. Assuming that τ_q is the same as the momentum relaxation time we obtain a hole mobility $\mu_h = 1.2 \pm 0.1 \text{ m}^2/\text{Vs}$. The dHvA amplitude calculation for electrons (Sec. III B 1) gave a mobility of $\mu_e = 6.7 \pm 0.4 \text{ m}^2/\text{Vs}$. The product of these two mobilities, $8.0 \pm 0.8 \text{ m}^4 (\text{Vs})^{-2}$, is consistent with the value obtained from the low-field curvature of R_{xx} .

IV. CONCLUSIONS

We have carried out Hall, SdH, and dHvA measurements on the same sample of HOPG, at temperatures down to 30 mK. Our Hall effect experiments confirm the carrier types established by Ref. 13: holes near the H point of the graphite Brillouin zone are responsible for the low-frequency component of the dHvA oscillations, while electrons at K give rise to the high-frequency component. Analyses of the Hall, dHvA, and SdH effects all indicate that the holes are subject to stronger scattering than the electrons. The origin of this observation will be the subject of further investigations of various types and grades of graphite. The temperature dependence of the dHvA effect indicates that the holes have larger Landau-level separations than the electrons, a conclusion confirmed by amplitude analyses of dHvA and SdH oscillations.

The analysis of the phase of the dHvA and SdH oscillations suggests that the low-frequency carriers (holes) are SFs, in agreement with the previous studies summarized in Table I and Fig. 2. The phases are consistent with the holes being two-dimensional, in agreement with the HOPG experiments of Ref. 6 but not with other experiments. This suggests that the interaction between atomic layers might be different in the different samples used. The situation with the high-frequency carriers (electrons) is more complicated. Our results show an intermediate value of the phase, consistent with neither DF nor SF. Other authors^{6,15} have also reported an intermediate phases for the high-frequency carrier. It is interesting to note that Ref. 4 pointed out that intermediate phases are possible for minority holes in situations close to magnetic breakdown, though this could not occur for majority carriers with standard values of the SW parameters. Intermediate phases might also be the result of sample inhomogeneity, in which electrons are SF and DF in different parts of the same sample, perhaps due to the presence of crystallites of different orientations within the plane or different stacking between planes. It is not clear why this should affect electrons more than holes though. Clearly graphite remains an interesting and intriguing material and more measurements on a range of graphite samples are needed in order to determine the nature of its electronlike quasiparticles.

*Deceased.

¹N. B. Brandt, S. M. Chudinov, and T. G. Ponomarev, *Semimetals: Graphite and its Compounds* (Elsevier Science Ltd., New York, 1988).

²I. A. Luk'yanchuk and Y. Kopelevich, *Phys. Rev. Lett.* **93**, 166402 (2004).

³I. A. Luk'yanchuk and Y. Kopelevich, *Phys. Rev. Lett.* **97**, 256801 (2006).

- ⁴G. P. Mikitik and Y. V. Sharlai, *Phys. Rev. B* **73**, 235112 (2006).
- ⁵M. Orlita, C. Faugeras, G. Martinez, D. K. Maude, M. L. Sadowski, and M. Potemski, *Phys. Rev. Lett.* **100**, 136403 (2008).
- ⁶J. M. Schneider, M. Orlita, M. Potemski, and D. K. Maude, *Phys. Rev. Lett.* **102**, 166403 (2009).
- ⁷I. A. Luk'yanchuk and Y. Kopelevich, *Phys. Rev. Lett.* **104**, 119701 (2010).
- ⁸J. M. Schneider, M. Orlita, M. Potemski, and D. K. Maude, *Phys. Rev. Lett.* **104**, 119702 (2010).
- ⁹J. C. Slonczewski and P. R. Weiss, *Phys. Rev.* **109**, 272 (1958).
- ¹⁰J. W. McClure, *Phys. Rev.* **108**, 612 (1957).
- ¹¹D. Shoenberg, *Philos. Trans. R. Soc. London A* **245**, 1 (1952).
- ¹²T. G. Berlincourt and M. C. Steele, *Phys. Rev.* **98**, 956 (1955).
- ¹³P. R. Schroeder, M. S. Dresselhaus, and A. Javan, *Phys. Rev. Lett.* **20**, 1292 (1968).
- ¹⁴D. E. Soule, J. W. McClure, and L. B. Smith, *Phys. Rev. A* **134**, A453 (1964).
- ¹⁵S. J. Williamson, S. Foner, and M. S. Dresselhaus, *Phys. Rev.* **140**, A1429 (1965).
- ¹⁶I. M. Lifshitz and A. M. Kosevich, *Sov. Phys. JETP-USSR* **2**, 636 (1956).
- ¹⁷J. A. Woollam, *Phys. Rev. B* **3**, 1148 (1971).
- ¹⁸K. S. Novoselov, A. K. Geim, S. V. Morozov, D. Jiang, Y. Zhang, S. V. Dubonos, I. V. Grigorieva, and A. A. Firsov, *Science* **306**, 666 (2004).
- ¹⁹K. S. Novoselov, A. K. Geim, S. V. Morozov, D. Jiang, M. I. Katsnelson, I. V. Grigorieva, S. V. Dubonos, and A. A. Firsov, *Nature (London)* **438**, 197 (2005).
- ²⁰Y. B. Zhang, Y. W. Tan, H. L. Stormer, and P. Kim, *Nature (London)* **438**, 201 (2005).
- ²¹A. J. Matthews, A. Usher, and C. D. H. Williams, *Rev. Sci. Instrum.* **75**, 2672 (2004).
- ²²A. Usher and M. Elliott, *J. Phys.: Condensed Matter* **21**, 103202 (2009).
- ²³T. Ando and T. Nakanishi, *J. Phys. Soc. Jpn.* **67**, 1704 (1998).
- ²⁴L. Smrčka and N. A. Goncharuk, *Phys. Rev. B* **80**, 73403 (2009).
- ²⁵A. A. Abrikosov, *Foundations of the Theory of Metals* (North Holland, Amsterdam, 1988).